Title:

The Berrettini palmar neural anastomosis: a study of 27 cadaveric specimens and determination of a high-risk surgical zone

Authors:

Akos Marton[1]; Shahzaib Ahmed[1]; Gavin E. Jarvis[1]; Cecilia Brassett[1]; Ian Grant[1,2]; Michael E. Gaunt[1]

Institutions:

1. Human Anatomy Centre, Department of Physiology, Development and Neuroscience, University of Cambridge, Cambridge, UK
2. Department of Plastic and Reconstructive Surgery, Addenbrooke's Hospital, Cambridge, UK

Corresponding author:

Akos MARTON

Human Anatomy Teaching Group

Department of PDN, University of Cambridge

Downing Site

Cambridge, CB2 3DY

United Kingdom

Email: am2485@cam.ac.uk / akosmarton97@gmail.com

Phone: +44(0)7565207637

Keywords: anatomical study, median nerve, ulnar nerve, Berrettini anastomosis

Acknowledgements: The authors would like to express their sincerest gratitude to the donors without whose generous gift this project could not have been possible. We would like to acknowledge the help and support of Maria Wright, James Skeates and Darren Broadhurst, dissection room staff of the Cambridge University Anatomy Department.

Declaration of conflicting interests: The authors declare no potential conflicts of interest with respect to the research, authorship, and/or publication of this article.

Funding statement: This work was funded by the University of Cambridge.

Ethical approval declaration: Ethical approval was not sought for the present study.

Informed consent declaration: Written consent was obtained from all donors before decease for the use of their bodies for anatomical research, in compliance with the Human Tissue Act (2004).

Contributorship details: All authors made a substantial contribution to the concept, design, data analysis and interpretation; drafting the article and revising it critically for important intellectual content; gave approval for the final version to be published; have participated sufficiently in the work to take public responsibility for the content.

The Berrettini palmar neural anastomosis: a study of 27 cadaveric specimens and determination of a high-risk surgical zone

ABSTRACT

In this cadaveric study, we analysed digital images of dissected palms to define the location and length of superficial anastomoses between the median and the ulnar nerves (Berrettini anastomoses). We found the anastomosis present in 12 of 27 hands. We used a coordinate model to define their location relative to seven specified landmarks. The model revealed that the Berrettini anastomosis was positioned consistently and we defined a high-risk zone in the palm that contained the majority of the anastomoses with a fraction projecting beyond the borders of the zone. We conclude that this high-risk zone in the palm can be of some help to reduce the risk of iatrogenic nerve injury, however, any operation in the palm must always be done with great care to visualize and protect any possible anatomically unusual structures.

INTRODUCTION

Anastomoses between the major nerves in the hand are a potential cause of clinical and neurophysiological misdiagnosis and a site of injury during hand surgery. The Berrettini anastomosis (BA) is an ulnar-median sensory nerve anastomosis with a reported prevalence of 60% (Roy et al., 2016). With its superficial position and close relation with the flexor retinaculum, it is particularly vulnerable to iatrogenic injury (Roy et al., 2016) (Figure 1a,b). While the BA is usually clinically silent, it may be associated with atypical patterns of sensory innervation leading to a complex neurological assessment and unexpected patterns of sensory disturbance (Seidel et al., 2020; Stopford, 1918). A recent meta-analysis highlighted a wide variance of data in reported prevalence of this anastomosis, possibly due to different study methodologies and reporting parameters, and recommended standardised reporting standards for future studies (Roy et al., 2016).

Computer-based modelling of high quality digital images can facilitate detailed anatomical investigation and analysis. In most studies of the BA, computer- and/or image-based methods for taking and analysing measurements have not been used.

In this cadaveric study, we report the prevalence, length and angle of the BA, and employ digital image analysis technology, coordinate data transformation and statistical modelling to define quantitatively the anatomy of the BA and establish a high-risk dissection zone that best reflects the location of the BAs.

METHODS

Specimens

Twenty-seven hands were obtained from donors embalmed using a 4.2% formaldehyde solution. One hand from each donor was selected for dissection, giving a sample of 13 right and 14 left hands. Donors were from the catchment area of the University of Cambridge, England, UK as defined by the Human Tissue Authority (https://www.hta.gov.uk/medical-schools) and all had provided written consent to the use of their bodies in anatomical research. (Donor information is found in Supplementary Table S1.)

Dissection and measurements

Superficial dissection of the palm was performed to achieve unrestricted access to the palmar branches of the ulnar and median nerves. After skin removal, the relevant neurovascular structures were dissected and identified. A communicating branch between two nerves was identified as a BA if the two endpoints were superficial palmar branches of the ulnar and median nerves (Figure 1a,b).

In those hands, in which a BA was identified, high quality digital photographs were taken. In each case, a ruler, elevated to level of the palmar plane, was in the frame to aid subsequent calibration.

The length and angle (defined as the angle between the common digital nerve from which it arises and the BA branch) were measured from the digital photographs using ImageJ image analysis software (v.1.52a, National Institutes of Health, Bethesda, MD, USA). ImageJ was calibrated to convert pixels to millimetres using the in-frame ruler.

Constructing a coordinate model.

A coordinate model of the hand was constructed to define the location of the BA within the palm using the digital images. The X dimension was from proximal to distal, and the Y dimension from ulnar to radial. The pisiform was defined as the origin (0,0, landmark 0) and the coordinate values were in mm. X,Y coordinates for the two endpoints of the BA on ulnar (bu) and radial (br) sides, and that of seven fixed landmarks (0 to 6) defining the hand perimeter were obtained from each hand (Figure 1c). These were the raw coordinates (X_{raw},Y_{raw}). Landmarks 0 to 6 were defined as follows:

0: Ulnar border of pisiform bone

1: Radial border of wrist

2: Base of the index finger at the level of palmar digital crease

3: Midpoint of skin margin in second web space

4: Midpoint of skin margin in third web space

5: Midpoint of skin margin in fourth web space

6: Ulnar border of the little finger at the level of palmar digital crease

Superimposition of the raw coordinates did not result in an optimised inter-subject anatomical comparison (Supplementary Figure S1a). To eliminate the inter-subject differences in size and rotation in the digital photographs, and thus achieve an optimised model, raw coordinates were subject to three transformations ensuring the original anatomical proportions of each hand are preserved.

The transformations were performed as follows (photographs of left hands were used as they were, whilst photographs of right hands were mirrored, and all the coordinates were treated as if from left hands):

1. For each hand, the mean of the *X* and *Y* coordinates for the seven anatomical landmarks ($\bar{x}_{l,raw}$ and $\bar{y}_{l,raw}$), were subtracted from each of the seven fixed and two BA landmarks to generate a new set of nine coordinates (termed: X_{t1},Y_{t1}). This has the effect of shifting the origin from the pisiform (landmark 0) to a location in the centre of the palm, such that $\bar{x}_{l,t1} = \bar{y}_{l,t1} = 0$. This transformation is independent in each hand and the resulting coordinates are shown in Supplementary Figure S1b.
2. The X_{t1},Y_{t1} coordinates in each hand were subject to a rotational transformation centred on the origin ($\bar{x}_{l,t1}$,$\bar{y}_{l,t1}$) using a rotation matrix such that:

   $$\begin{bmatrix} x_{t2} \\ y_{t2} \end{bmatrix} = \begin{bmatrix} \cos\theta & -\sin\theta \\ \sin\theta & \cos\theta \end{bmatrix} \begin{bmatrix} x_{t1} \\ y_{t1} \end{bmatrix}$$

   where θ is a variable parameter equal to the anti-clockwise rotational angle, and is constant within a hand but varies between hands. The effect of this transformation is to rotate the images of the hands so that they were aligned as closely as possible, as defined by the objective function (see below). The resulting coordinates are shown in Supplementary Figure S1c.
3. The X_{t2},Y_{t2} coordinates in each hand were subject to a scalar transformation of the form:

   $$\begin{bmatrix} x_{t3} \\ y_{t3} \end{bmatrix} = S \begin{bmatrix} x_{t2} \\ y_{t2} \end{bmatrix}$$

   where *S* is a variable parameter equal to the unidimensional fold change brought about by the transformation. It is constant within a hand and varies between hands. The effect of this transformation is to scale the images of the hands up or down so that they were aligned as closely as possible, as defined by the objective function (see below). The resulting coordinates are shown in Supplementary Figure S1d.

Unique values of Θ and S were estimated for each hand such that $\bar{\Theta}$ = 0, and $\bar{S}$ = 1, meaning that across all hands there was no net rotation and no net change in scale. N - 1 values of Θ and of S were estimated: the remaining non-estimated value of Θ was constrained to equal the negative sum of the 11 estimated Θs, and the non-estimated value of S was constrained to equal 12 minus the sum of the estimated 11 Ss.

Parameter estimates of Θ and S were obtained by minimising an objective function (OBJ). This was the sum across all hands (n = 12) of the squared deviations from the mean for the seven paired landmark coordinates ($X_{l.t3}$,$Y_{l,t3}$) within each hand as follows:

$$OBJ = \sum_{j=1}^{12} \left(\sum_{i=0}^{6} \left(x_{i,t3} - \overline{x}_{l,t3} \right)^2 + \sum_{i=0}^{6} \left(y_{i,t3} - \overline{y}_{l,t3} \right)^2 \right)$$

Where: j indicates each hand; i indicates each fixed anatomical landmark.

Minimisation was performed using the Solver function in Microsoft Excel. Post-minimisation, OBJ = 773.0, and the estimates of the parameters for each hand are shown in Supplementary Table S2. In effect, the transformations generated a coordinate map for a rotationally- and size-standardised hand. The coordinate values (mean ± SD) for the seven landmarks are illustrated in Supplementary Figure S1.

For each hand, using the values in Supplementary Table S2, the three transformations were applied to the raw BA coordinates to obtain new coordinates that mapped onto the standardised hand. The resulting coordinates were: $\bar{x}_{bu,t3}$ = -35.1 ± 6.8 $\bar{y}_{bu,t3}$ = -9.6 ±

3.3 and $\bar{x}_{br,t3}$ = -19.9 ± 6.1 $\bar{y}_{bu,t3}$ = -0.5 ± 2.8. Supplementary Figure S1d shows the final model.

The transformations resulted in a graphical model that shows the defined anatomical landmarks and BAs from each hand superimposed and readily comparable (Figure 2). This model was used to identify a high-risk dissection zone in the palm. Potential definitions of such a zone based on the defined anatomical landmarks were assessed and the number of BA endpoints within proposed zones compared. Each zone was defined by four points: two points along the line between landmarks ‘0’ and ‘2’, and two points along the line between landmarks ‘0’ and ‘4’ (Figure 1c). The location of the four points along the lines ranged from 0% to 100% of total distance, in 5% increments. The number of anatomical endpoints – of a total of 24 endpoints from 12 BAs – contained within each of the potential zones were assessed to identify the most comprehensive and anatomically-minimised definition of the high-risk zone (Supplementary Figure S2a-b).

Statistics

Confidence intervals for proportions were calculated using the modified Wald method. Length and angle values are shown with standard deviation (SD) estimates throughout. Associations between the presence of a BA and either sex or side were evaluated using Fisher’s Exact Test (FET). Two-tailed *P* values are reported.

RESULTS

The BA was identified in 12 of 27 hands (0.44, 95% CI [0.28, 0.63]), being present in 6/13 (0.46, 95% CI [0.23, 0.71]) male specimens and 6/14 (0.43, 95% CI [0.21, 0.67]) female specimens (p=1.0). More BAs were found in right (9/13;0.69 95% CI [0.42, 0.88]) compared to left (3/14;0.21 95% CI [0.07, 0.48]) hands (p=0.021) (Supplementary Table S1).

The mean length of the BA was 20 mm (SD 5, range: 10-31mm). The mean angle between the communicating branch and the nerve trunk of origin was 29° (SD 15, range: 17-61°) (Supplementary Table S3). We observed two cases where the BAs enclosed angles larger than 45°: 54° (Specimen no.7) and 61° (Specimen no.12).

The graphical model from the coordinate data transformation showed clustering of the BAs in a small region in the hand. We assessed 231 potential zones to define a high-risk dissection zone that best reflects the location of the BAs (Supplementary Figure S2). The most inclusive yet smallest high-risk zone was the area between the four points at 20% and 60% of total distance along the lines between landmarks ‘0’ and ‘2’ or ‘4’, (Figure 2). This contained 22/24 endpoints of the 12 BAs.

A clinically more easily adoptable version of the high-risk dissection zone, or “danger zone” was defined using 25% and 50% of the total distance along the two lines (Figure 2). In the model, this contained 19/24 endpoints of the 12 BAs and 8/12 full-length BAs. The “danger zone” can be found using the following steps:

1. Locate the ulnar border of the pisiform.

2. Draw a line from the ulnar border of the pisiform to the radial border of the base of the index finger at the level of the palmar digital crease. Mark the halfway point along that line, then the halfway point along the proximal half-segment.
3. Draw another line from the ulnar border of the pisiform to the skin margin in the third web space between the middle and ring fingers. Mark the halfway point along this line, then the halfway point along the proximal half-segment.
4. The quadrilateral defined by these four marked points outlines a “danger zone” where the BA is likely to be found if present.

This 25%-50% procedure was applied to each photograph of the 12 hands, thereby mimicking a pre-surgical evaluation in an individual patient. In 7/12 hands the BA lay fully within the “danger zone” and 18/24 endpoints were within the same zone, with minimal projection beyond the border of the zone.

DISCUSSION

This study investigated the anatomy of the Berrettini anastomosis (BA) within a convenience sample of cadavers drawn from a geographical area surrounding Cambridge, UK, focusing on its prevalence and location in the palm. We confirmed that the BA is a common variant, and our statistical modelling enabled us to define an easily identifiable zone where the BA is likely to be found, if present.

The prevalence in our sample (44%) was in the lower mid-range of reported prevalence in the literature. The average reported in the literature is 61%, with marked variability in the results of other authors, ranging from 4% to 96% (Bas and Kleinert, 1999; Don Griot et al., 2000; Ferrari and Gilbert, 1991; Hoogbergen and Kauer, 1992; Loukas et al., 2007; Meals and Shaner, 1983; Olave et al., 2001; Roy et al., 2016; Stančić et al., 1999; Sulaiman et al., 2016; Tagil et al., 2007; Zolin et al., 2014). This wide range may be caused by a variety of reasons related to differing methods of dissection and reporting standards. The high occurrence of BA in the hand observed here and by other authors suggests that this anastomosis is not a rare anatomical variant and may be considered more of a normal "mingling" of the fibres of the ulnar and median nerves.

Roy et al. (2016) recommended a standardised classification system for future studies, comprising three types of BAs based on their transverse orientation. In the current study, all BAs that we dissected were in an ulnar to median orientation. The mean length was 20 mm (SD 5.5), consistent with reports in the literature. The meta-analysis by Roy et al. (2016) reported a mean length of 19.47 mm (SD 8.766) in 63 upper limbs). The mean angle between the communication and its nerve branch of origin was 29° (SD 15Communicating branches that course at a close-to-perpendicular angle have been proposed to be at higher risk of being severed during surgery (Ferrari and Gilbert, 1991). Procedures with the greatest risk of iatrogenic injury include open and endoscopic carpal tunnel release, ring finger flexor tendon surgery, Dupuytren's fasciectomy, and mobilisation of neurovascular island flaps (Loukas et al., 2007).

A well-defined "danger zone" could assist surgeons in estimating where a communicating branch intra-operatively may lie. Previous descriptions of such a region were defined with reference to variable soft tissue surface landmarks, such as wrist and palmar creases (Ferrari and Gilbert, 1991; Loukas et al., 2007; Sulaiman et al., 2016), or to deep bony landmarks which are not always easily identifiable, such as the styloid processes of the ulnar and radial bones and the metacarpophalangeal joints (Don Griot et al., 2000).

We defined a high-risk zone for dissection in terms of distances along the lines from the pisiform to the bases of the index and ring fingers. A large set of potential definitions of this zone were assessed. When assessing how many endpoints were contained in each of these potential zones, we found that the smallest yet most inclusive definition of the high-risk zone was at 20% and 60% of the total distances along both lines, containing 22 of 24 endpoints of the 12 BAs. In addition to the 'optimal' 20%-60% high-risk zone, we defined a 25%-50% "danger zone", which in our clinical judgement is easier to adopt in practice, containing seven BAs completely and the majority of the length of the remaining five BAs within the zone. Our proposed definition of the "danger zone" has two advantages over previous ones. Firstly, it is defined in terms of standardised distances measured from the ulnar vertex of the pisiform, which is an easily palpable bony landmark and constant reference point. Secondly, it was defined using a quantitative approach that simplifies considerably the illustration of this anatomical variant and provides a method for reproducible numerical analysis. We propose this method may be used to report anatomical variation in future studies.

This study has some limitations. The sample size was small, with 27 hands dissected in total, and the BA identified in 12 of these. Such small sample, in conjunction with the inherently variable anatomy of the BA nerve connection, will limit the gravity of the above results when translated into clinical practice. Furthermore, the number of BAs that lie partly outside of the proposed "danger zone" is not insignificant. Whilst the proposed high-risk dissection zone can provide rough guidance, it is not intended to be a definitive representation of where the BA is located. Regardless of this, dissection in the palm must always be done with great care to identify and protect possible anatomically unusual structures such as the BA.

REFERENCES

Bas H, Kleinert JM. Anatomic variations in sensory innervation of the hand and digits. J Hand Surg Am. 1999, 24: 1171–84.

Don Griot JPW, Zuidam JM, Van Kooten EO, Prosé LP, Hage JJ. Anatomic study of the ramus communicans between the ulnar and median nerves. J Hand Surg Am. 2000, 25: 948–54.

Ferrari GP, Gilbert A. The superficial anastomosis on the palm of the hand between the ulnar and median nerves. J Hand Surg Am. 1991, 16: 511–4.

Hoogbergen MM, Kauer JMG. An unusual ulnar nerve-median nerve communicating branch. J Anat. 1992, 181: 513–6.

Loukas M, Louis RG, Stewart L, et al. The surgical anatomy of ulnar and median nerve communications in the palmar surface of the hand. J Neurosurg. 2007, 106: 887–93.

Meals RA, Shaner M. Variations in digital sensory patterns: A study of the ulnar nerve—median nerve palmar communicating branch. J Hand Surg Am. 1983, 8: 411–4.

Olave E, Del Sol M, Gabrielli C, Mandiola E, Rodrigues CFS. Biometric study of the relationships between palmar neurovascular structures, the flexor retinaculum and the distal wrist crease. J Anat. 2001, 198: 737–41.

Roy J, Henry BM, PĘkala PA, et al. Median and ulnar nerve anastomoses in the upper limb: A meta-analysis. Muscle and Nerve. 2016, 54: 36–47.

Seidel GK, Seidel ME, Hakopian D, et al. Frequency of Electrodiagnostically Measurable Berrettini Anastomosis. J Clin Neurophysiol. 2020, 37: 214–9.

Stančić MF, Mićović V, Potočnjak M. The anatomy of the Berrettini branch: Implications for carpal tunnel release. J Neurosurg. 1999, 91: 1027–30.

Stopford JS. The Variation in Distribution of the Cutaneous Nerves of the Hand and Digits. J Anat. 1918, 53: 14–25.

Sulaiman S, Soames R, Lamb C. An anatomical study of the superficial palmar communicating branch between the median and ulnar nerves. J Hand Surg Eur. 2016, 41: 191–7.

Tagil SM, Bozkurt MC, Özçakar L, Ersoy M, Tekdemir I, Elhan A. Superficial palmar communications between the ulnar and median nerves in Turkish cadavers. Clin Anat. 2007, 20: 795–8.

Zolin SD, Barros MD, Abdouni YA, Nascimento VDG, Costa AC Da, Chakkour I. Anatomical study of sensory anastomoses in the hand. Acta Ortop Bras. 2014, 22: 34–7.

FIGURE LEGENDS

Figure 1. (a) Specimen no .6 with the Berrettini anastomosis present (arrow). (b) Schematic drawing showing the anatomy of the same specimen. (c) Schematic drawing showing the landmarks measured using ImageJ. Landmarks ‘0’: Ulnar border of pisiform bone; ‘1’: Radial border of wrist; ‘2’: Base of the index finger at the level of palmar digital crease; ‘3’: Midpoint of skin margin in second web space; ‘4’: Midpoint of skin margin in third web space; ‘5’: Midpoint of skin margin in fourth web space; ‘6’: Ulnar border of the little finger at the level of palmar digital crease; ‘bu’: Ulnar endpoint of Berrettini anastomosis; ‘br’: Radial endpoint of Berrettini anastomosis. P: pisiform bone

Figure 2. The hand model after the transformations. The landmarks and the BAs from all 12 hands with the BA are shown. The zones according to the 25%-50% and the 20%-60% definitions are shown.

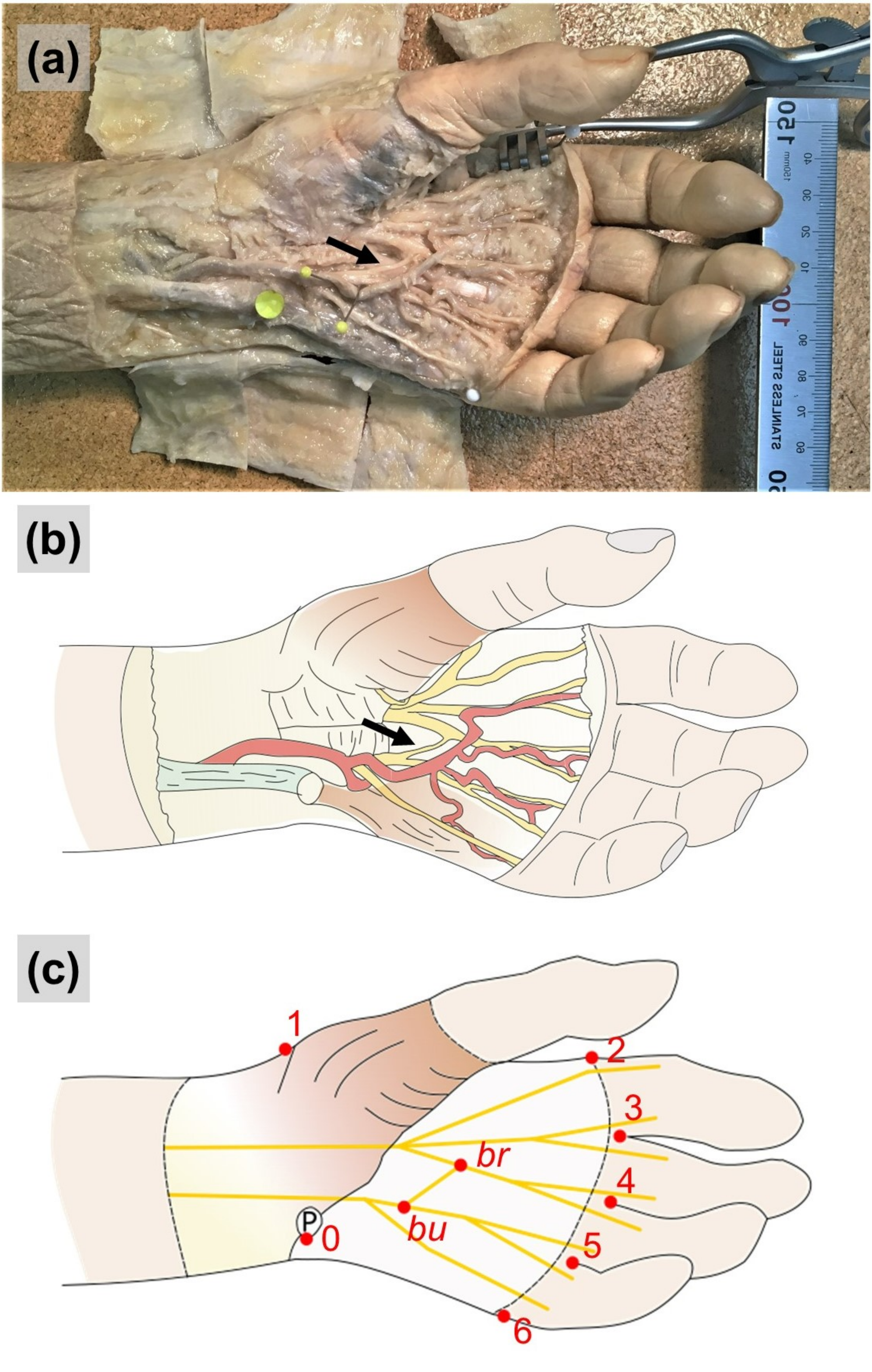
(a)
(b)
(c)
1
2
3
4
5
6
0
P
br
bu

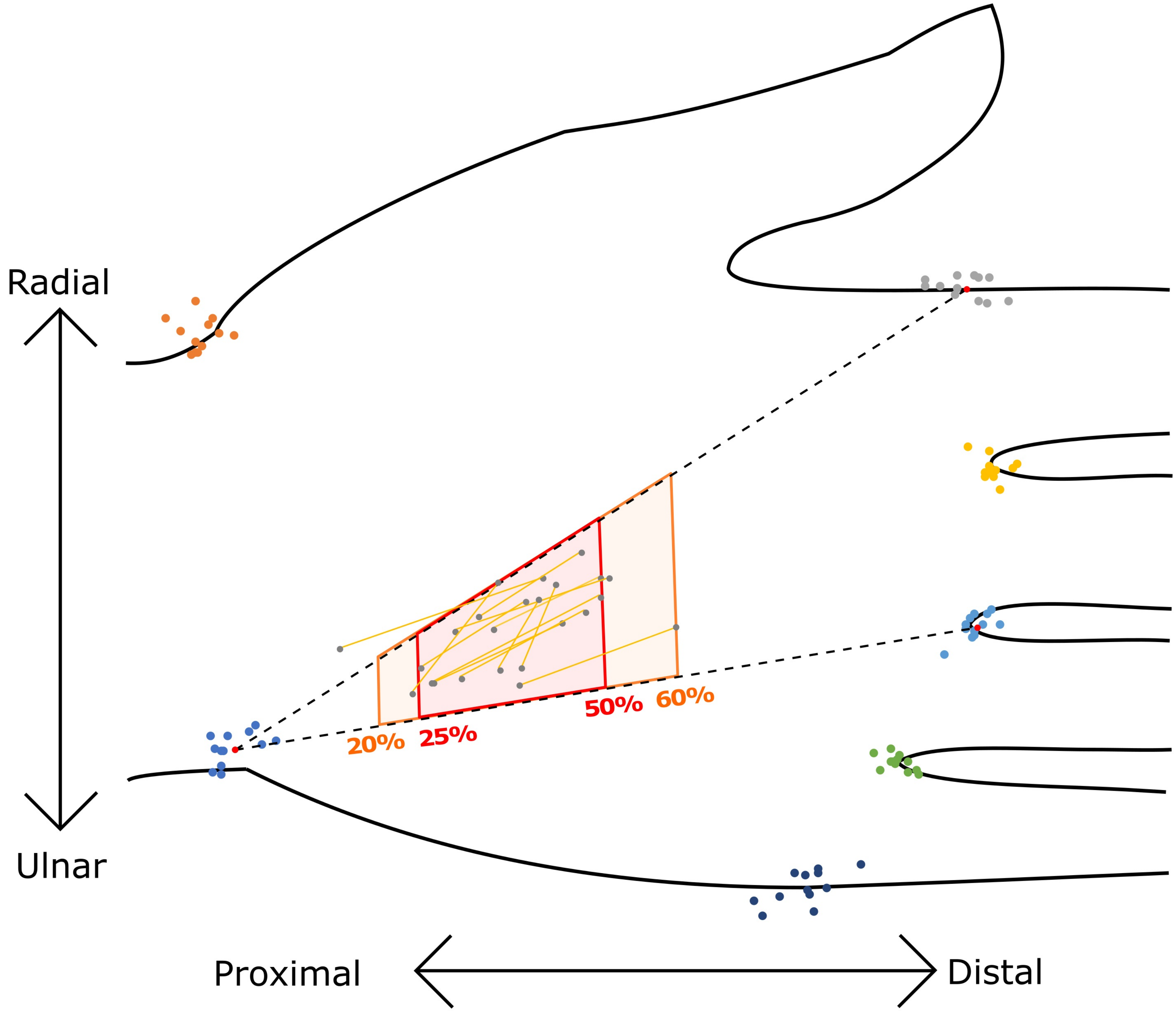

Radial
Ulnar
20%
25%
50%
60%
Proximal
Distal

Specimen no.	Sex	Age	Side	Berrettini present?
1	M	48	R	Yes
2	M	75	R	Yes
3	F	92	R	Yes
4	F	85	R	Yes
5	M	80	L	Yes
6	F	94	R	Yes
7	F	93	R	Yes
8	M	87	R	Yes
9	M	96	R	Yes
10	M	83	L	Yes
11	F	87	L	Yes
12	F	87	R	Yes
13	M	90	L	No
14	M	75	L	No
15	M	90	R	No
16	F	86	R	No
17	F	92	L	No
18	M	87	L	No
19	M	94	L	No
20	M	87	R	No
21	F	77	L	No
22	F	94	R	No
23	F	100	L	No
24	F	93	L	No
25	F	89	L	No
26	F	104	L	No
27	M	74	L	No

Supplementary Table S1. Demographic data of donors, laterality of the dissected hand, and the presence on the Berrettini anastomosis. M: male, F: female, L: left, R: right

Hand	***X* shift (mm)**	***Y* shift (mm)**	***Θ* (degrees)**	***S***
1	-74.6	-25.8	-2.80	0.881
2	-67.1	-18.9	2.35	0.985
3	-61.3	-24.9	-5.35	1.021
4	-61.0	-13.9	4.16	1.032
5	-69.1	-26.3	-1.18	0.939
6	-55.4	-14.2	4.52	1.082
7	-54.4	-20.0	-1.43	1.098
8	-70.9	-23.4	1.66	0.949
9	-59.5	-9.4	7.43	1.052
10	-70.8	-29.9	-2.32	0.908
11	-60.0	-24.2	-4.43	1.075
12	-65.4	-24.9	-2.61	0.978
mean ± SD	**-64.1 ± 6.5**	**-21.3 ± 6.1**	**0.00 ± 3.96**	**1.000 ± 0.071**

Supplementary Table S2. Post-minimisation estimates of the parameters for each hand.

Specimen no.	Length (mm)	P-B1 (mm)	P-B2 (mm)	Angle (degrees)
1	30.8	23.0	53.9	16.7
2	23.0	39.5	62.0	20.6
3	18.8	36.0	51.4	22.6
4	18.3	24.2	41.0	16.6
5	21.7	35.8	55.0	25.4
6	20.3	26.4	43.8	17.1
7	9.8	33.1	39.5	54.0
8	25.7	34.4	59.1	17.0
9	20.7	26.1	46.9	21.9
10	12.0	42.2	51.5	39.0
11	20.1	27.5	42.3	30.6
12	18.7	26.2	42.3	60.5

Supplementary Table S3. Results of the measurements. P-B1 and P-B2 represent the distance between the ulnar vertex of the pisiform bone and the proximal and distal ends of the Berrettini anastomosis respectively.

Fig. S1a: Raw coordinates (X_{raw},Y_{raw})

mean ± SD (*raw*)

Landmark (*i*)	x_i	y_i
0	0 ± 0	0 ± 0
1	-4.2 ± 3.4	54.5 ± 5.4
2	95.6 ± 10.6	60.9 ± 9.9
3	99.2 ± 8.7	37.0 ± 9.7
4	96.9 ± 8.8	16.3 ± 8.4
5	86.7 ± 7.6	-1.6 ± 6.9
6	74.7 ± 10.1	-17.9 ± 5.7
bu	28.8 ± 6.3	11.5 ± 4.0
br	44.1 ± 7.8	20.5 ± 5.8

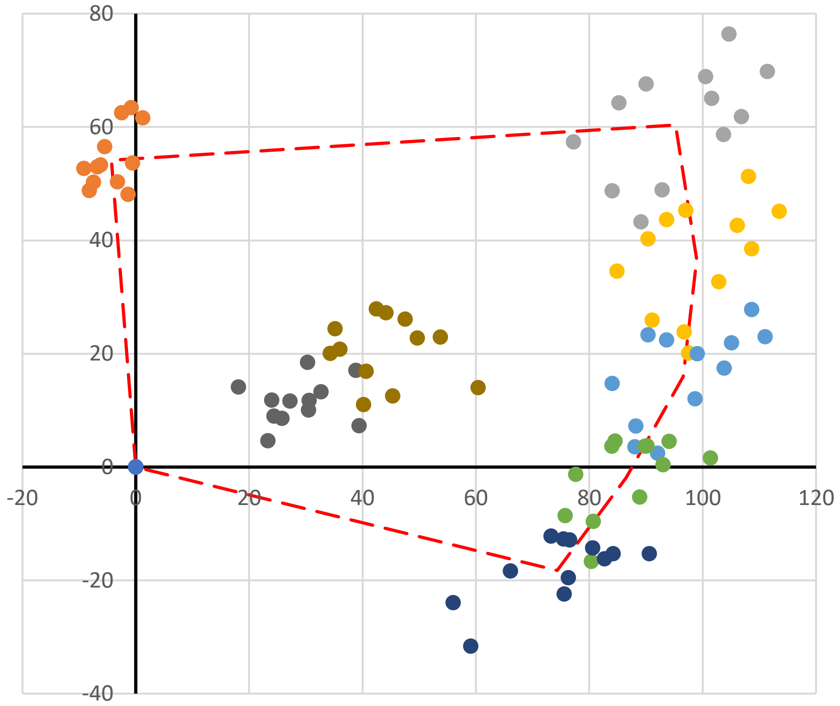

Fig. S1b: Transformation 1 ($t1$) (X_{t1},Y_{t1})
Origin shift

mean ± SD ($t1$)

Landmark (i)	x_i	y_i
0	-64.1 ± 6.5	-21.3 ± 6.1
1	-68.3 ± 5.3	33.2 ± 5.0
2	31.5 ± 4.6	39.6 ± 3.9
3	35.1 ± 3.1	15.7 ± 3.8
4	32.8 ± 3.0	-5.0 ± 2.7
5	22.6 ± 2.0	-22.9 ± 1.8
6	10.6 ± 5.3	-39.2 ± 2.3
bu	-35.4 ± 8.5	-9.9 ± 4.5
br	-20.0 ± 6.5	-0.8 ± 2.8

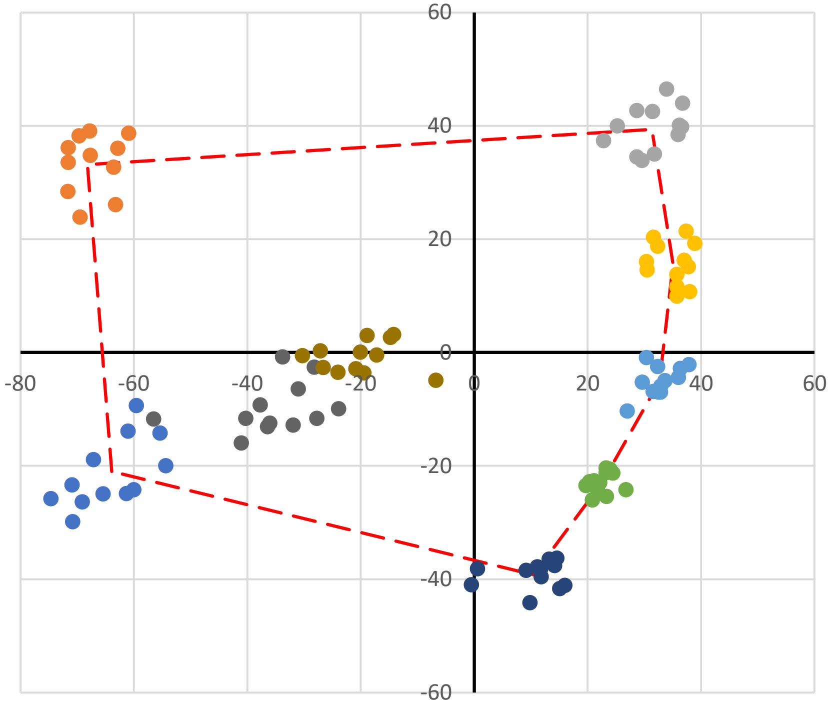

Fig. S1c: Transformation 2 ($t2$) (X_{t2},Y_{t2})
Rotation

mean ± SD ($t2$)

Landmark (i)	x_i	y_i
0	-64.3 ± 6.9	-21.2 ± 3.2
1	-68.5 ± 4.6	33.3 ± 2.6
2	31.6 ± 5.1	39.5 ± 2.6
3	35.2 ± 2.7	15.7 ± 2.1
4	32.8 ± 2.9	-5.0 ± 1.5
5	22.6 ± 1.3	-23.0 ± 1.5
6	10.6 ± 3.9	-39.4 ± 2.5
bu	-35.5 ± 8.6	-9.7 ± 3.5
br	-20.0 ± 6.5	-0.5 ± 2.8

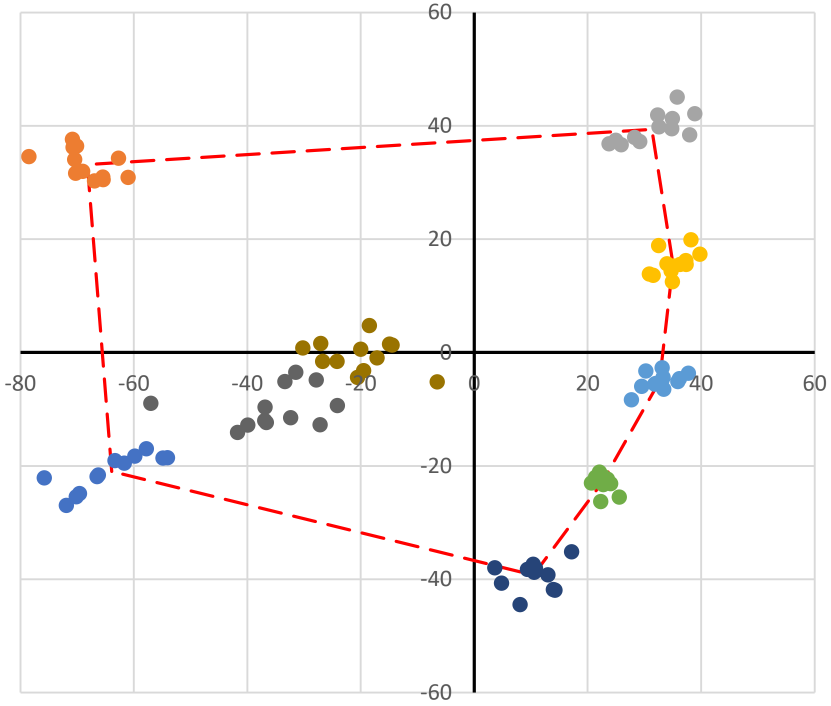

Fig. S1d: Transformation 3 (*t*3) (X_{t3},Y_{t3})
Scaling

mean ± SD (*t*3)

Landmark (*i*)	x_i	y_i
0	-63.9 ± 2.8	-21.0 ± 2.1
1	-68.2 ± 2.3	33.2 ± 2.2
2	31.3 ± 3.4	39.4 ± 1.4
3	35.1 ± 1.7	15.6 ± 1.5
4	32.7 ± 1.9	-5.0 ± 1.6
5	22.6 ± 1.8	-22.9 ± 1.0
6	10.5 ± 3.7	-39.3 ± 2.2
bu	-35.1 ± 6.8	-9.6 ± 3.3
br	-19.9 ± 6.1	-0.5 ± 2.8

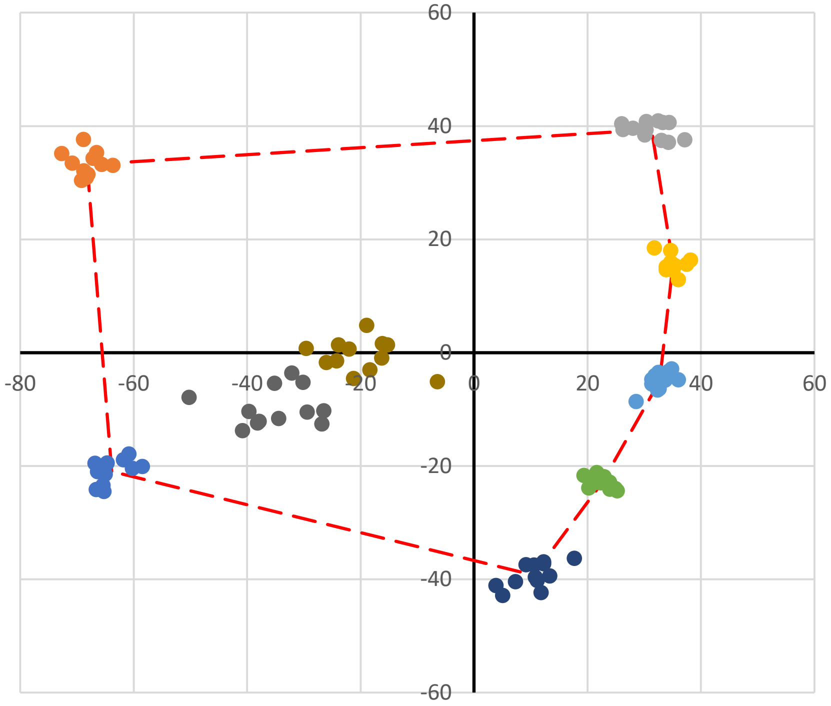

Fig. S2a: Model to assess potential high-risk zones. Upper and lower limits are the percentages of the total distance along both defined lines (landmarks 0→2 and landmarks 0→4). Values in cells are the number of endpoints contained in the zone according to each definition.

UPPER LIMIT -->	0%	5%	10%	15%	20%	25%	30%	35%	40%	45%	50%	55%	60%	65%	70%	75%	80%	85%	90%	95%	100%	<-- LOWER LIMIT
0%	0																					
5%	0	0																				
10%	0	0	0																			
15%	0	0	0	0																		
20%	0	0	0	0	0																	
25%	1	1	1	1	1	0																
30%	4	4	4	4	4	3	0															
35%	7	7	7	7	7	6	3	0														
40%	12	12	12	12	12	11	8	5	0													
45%	16	16	16	16	16	15	12	9	4	0												
50%	20	20	20	20	20	19	16	13	8	4	0											
55%	21	21	21	21	21	20	17	14	9	5	1	0										
60%	22	22	22	22	22	21	18	15	10	6	2	1	0									
65%	22	22	22	22	22	21	18	15	10	6	2	1	0	0								
70%	22	22	22	22	22	21	18	15	10	6	2	1	0	0	0							
75%	22	22	22	22	22	21	18	15	10	6	2	1	0	0	0	0						
80%	22	22	22	22	22	21	18	15	10	6	2	1	0	0	0	0	0					
85%	22	22	22	22	22	21	18	15	10	6	2	1	0	0	0	0	0	0				
90%	22	22	22	22	22	21	18	15	10	6	2	1	0	0	0	0	0	0	0			
95%	22	22	22	22	22	21	18	15	10	6	2	1	0	0	0	0	0	0	0	0		
100%	22	22	22	22	22	21	18	15	10	6	2	1	0	0	0	0	0	0	0	0	0	

Fig. S2b: An example of the zones defined in Supplementary Figure S2a where the zone is defined by the four points at 20% and 60% of total distance along the lines. It contains 22/24 BA endpoints.